INTERNATIONAL JOURNAL FOR NUMERICAL METHODS IN FLUIDS, VOL. 15, 729–741 (1992)

NUMERICAL SOLUTION OF THE VISCOUS STABILITY EQUATIONS FOR LOW-SPEED REACTING FLOWS

SHANKAR MAHALINGAM

Center for Combustion Research, Department of Mechanical Engineering, University of Colorado, Boulder, CO 80309-0427, U.S.A.

SUMMARY

The governing equations required to analyse the linear (viscous) stability of low-speed reacting flows are derived and a solution method based on initial value problems is described. The algorithm accurately reproduces the neutral stability curve for a non-reacting viscous shear layer, thus providing partial validation. The results for premixed and non-premixed flames in planar shear layers are presented and discussed.

KEY WORDS Linear stability Reacting flows Viscous theory

1. INTRODUCTION

In the past, several researchers have derived equations to study the linear stability of reacting flows to imposed small perturbations. Kimura[1] performed a stability analysis, which was later followed by Grant and Jones[2] to understand the flickering of a candle. Buckmaster and Peters[3] suggested improvements to account for gravity effects on the mean flow field. Trouve *et al.*[4] studied the linear stability of a premixed flame in a ramjet combustor. Mahalingam *et al.*[5] showed that inclusion of chemical reaction for the mean flow is crucial, but its neglect in the disturbance equations is a good first approximation. Jackson and Grosch[6] studied the stability of a supersonic reacting shear layer. In related works, variable density shear layer studies have been reported by Maslowe and Kelly[7] and Koochesfahani and Frieler.[8] In all these cases, the analyses have been inviscid. In typical flames, the local Reynolds number may be reduced significantly in the vicinity of reaction zones; hence, viscous effects are likely to be significant.

In the present paper, the necessary framework to investigate the effects of viscosity is developed in Section 2. To simplify the analysis and discussion of the solution procedure, constant viscosity is assumed. However, the technique is readily extended to include viscosity variation with temperature, as demonstrated in Section 4. The numerical procedure is described in Section 3. Asymptotic solutions are derived, and a method based on 'shooting' is discussed to solve the eigenvalue problem. A pseudo-orthogonalization procedure designed to maintain linear independence of the solutions during the integration process is also described. The method of contour integration is used to isolate multiple modes and simplify the search for eigenvalues. The results and conclusions are discussed in Sections 4 and 5, respectively. A comparison of the calculated neutral curve with the past results for a non-reacting shear layer provides partial validation of the proposed numerical method. High Reynolds number results obtained for premixed and non-premixed flames in shear layers are consistent with past inviscid results, providing further

0271–2091/92/180729–13$11.50

Received 22 April 1991
Revised 27 March 1992

validation of the method. Finally, the assumption of constant viscosity is relaxed and the numerical method is used to obtain the neutral curve for a non-premixed flame in a shear layer in which viscosity varies with temperature. The appropriate equations are summarized in Appendix A.

2. VISCOUS STABILITY EQUATIONS

The problem considered is premixed and non-premixed flames in two-dimensional planar shear layers. All flow variables are expressed as the sum of a mean and a disturbance component. Thus,

$$h(x, y, t)=\bar{h}(y)+h'(x, y, t), \tag{1}$$

where $h(x, y, t)$ is a generic flow variable that is a function of position and time. The overbars and primes indicate the mean and disturbance components, respectively. The predominant flow direction is assumed to be parallel to the x-axis. The parallel flow assumption is invoked. Thus, $\bar{h}$ is assumed to vary only with the cross-stream co-ordinate y. Since the focus is on low-speed flows, it is appropriate to use the low Mach number equations used by McMurtry *et al.*[9] and Mahalingam *et al.*[10] In subsequent sections, all dependent variables are dimensionless and are the zeroth- or first-order coefficients in an expansion in the square of the Mach number. The decomposition in equation (1) is substituted into the governing continuity, momentum and energy equations. The equations governing disturbance quantities are linearized by neglecting the products of disturbances. It is assumed that the terms corresponding to the reaction rate in the disturbance equations are small, except for their influence on the mean flow. Inviscid results of Mahalingam *et al.*[5] justify this approximation.

It is presumed that any general disturbance can be constructed by a proper superposition of wave-like disturbances. Thus,

$$h'(x, y, t)=\tilde{h}(y)\exp[\mathrm{i}(\alpha x-\beta t)] \tag{2}$$

Here α is the complex streamwise wavenumber, β the given temporal frequency, and i is defined by $\mathrm{i}\equiv\sqrt{(-1)}$. The quantity $\tilde{h}(y)$ is the eigenfunction. Amplified disturbances are obtained when α_i, the imaginary part of α, is negative. These grow exponentially with a growth rate $-\alpha_i$ at a phase velocity β/α_r. Substituting equation (2) in the disturbance equations, the following set of homogeneous equations are obtained. These are the continuity, x and y momentum, and energy equations, respectively: (In what follows in the rest of this paper, a prime indicates differentiation with respect to y.)

$$\mathrm{i}\tilde{\rho}(\alpha U-\beta)+\tilde{v}\rho'+\rho(\tilde{v}'+\tilde{u}\mathrm{i}\alpha)=0, \tag{3}$$

$$-\mathrm{i}\beta\rho\tilde{u}+\rho\tilde{v}U'+\rho U\mathrm{i}\alpha\tilde{u}=-\mathrm{i}\alpha\tilde{p}+\frac{\mu}{Re}(\tilde{u}''-\alpha^2\tilde{u}+\mathrm{i}\alpha\tilde{m}-\tfrac{2}{3}\tilde{m}\mathrm{i}\alpha), \tag{4}$$

$$-\mathrm{i}\beta\rho\tilde{v}+\rho U\mathrm{i}\alpha\tilde{v}=-\tilde{p}'+\frac{\mu}{Re}(\tilde{v}''-\alpha^2\tilde{v}+\tilde{m}'-\tfrac{2}{3}\tilde{m}'), \tag{5}$$

$$\mathrm{i}(\alpha U-\beta)\rho\tilde{T}+\rho T'\tilde{v}=\frac{k/c_p}{RePr}(\tilde{T}''-\alpha^2\tilde{T}), \tag{6}$$

where $\tilde{m}$ is defined as $\tilde{m}\equiv\mathrm{i}\alpha\tilde{u}+\tilde{v}'$. The symbols U, ρ and T represent the mean streamwise velocity, density and temperature, respectively. The quantities $\tilde{\rho}$, $\tilde{u}$, $\tilde{v}$ and $\tilde{T}$ represent the density, x and y velocity components, and the temperature eigenfunctions, respectively. The symbols μ, Re, Pr, k and c_p represent the dynamic viscosity, Reynolds number, Prandtl number, thermal

conductivity and specific heat, respectively. Equations (3)–(6) represent a system of six first-order differential equations, requiring six boundary conditions.

For the purposes of numerical solution, equations (3)–(6) are manipulated as follows. It is convenient to define the complex phase speed as

$$c \equiv \frac{\beta}{\alpha}. \tag{7}$$

Using the ideal gas equation of state, the density disturbance is eliminated from the continuity equation (3). The resulting equation is rewritten so that the highest derivative term appears on the left-hand side, yielding

$$\tilde{v}' = -i\alpha\tilde{u} + i\alpha\frac{\tilde{T}}{T}(U-c) - \frac{\rho'}{\rho}\tilde{v}. \tag{8}$$

Next, the pressure eigenfunction $\tilde{p}$ is eliminated from equations (4) and (5). Thus,

$$\tilde{u}''' = \frac{\rho Re i\alpha}{\mu}\left[(U-c)\tilde{u}' - i\alpha(U-c)\tilde{v} + U'\tilde{u} + \frac{\rho'}{\rho}(U-c)\tilde{u} + \frac{1}{i\alpha}\left(U'\tilde{v}' + U''\tilde{v} + \frac{\rho'}{\rho}U'\tilde{v}\right)\right] + \alpha^2\tilde{u}' - i\alpha^3\tilde{v} + i\alpha\tilde{v}''. \tag{9}$$

Since $\tilde{v}''$ appears on the right-hand side of equation (9), equation (8) is differentiated once (this increases the overall order of the equation) and written as

$$\tilde{v}'' = -i\alpha\tilde{u}' + i\alpha\frac{\tilde{T}}{T}U' + i\alpha\frac{\tilde{T}'}{T}(U-c) - i\alpha\frac{T'}{T^2}\tilde{T}(U-c) - \frac{\rho'\tilde{v}' + \tilde{v}\rho''}{\rho} + \frac{\rho'^2}{\rho^2}\tilde{v}. \tag{10}$$

Finally, equation (6) is rewritten as

$$\tilde{T}'' = \frac{RePr}{(k/c_p)}\rho[\tilde{T}i\alpha(U-c) + T'\tilde{v}] + \alpha^2\tilde{T}. \tag{11}$$

Note that equations (9)–(11) represent a system of seven first-order differential equations. Also, for constant density flows, ρ, T are constants, and $\tilde{T}=0$. Thus, equation (11) drops out. The resulting equations reduce to the classical fourth-order Orr–Sommerfeld equation for incompressible flow. The only mean flow information required in this limit is the velocity profile.

3. NUMERICAL SOLUTION PROCEDURE

Drazin and Reid[11] provide a comprehensive discussion of the various numerical methods used to solve the viscous stability equations. The methods are based on either an initial value problem or a boundary value problem method. The former methods are computationally less demanding in terms of computer memory and CPU time, and are flexible in that they adjust to the local character of the solution. However, they can be sensitive to the initial guess of the eigenvalue. The latter methods are based on reducing the system of differential equations to algebraic equations, using a finite difference or spectral discretization. A solution to the generalized eigenvalue problem that arises provides the required eigenvalues. As discussed by Malik,[12] these methods typically strain the resources of the computer.

In this paper, the eigenvalue problem described by equations (9)–(11) is solved by the 'shooting' method for initial value problems. Profile shapes for the mean velocity and temperature are prescribed. In the absence of analytical solutions for the laminar reacting flow problem, the

profiles are represented by analytical expressions that typify flames in shear layers. For specified Re, β and a guessed value of α, the equations are integrated from $y=\infty$ to $y=-\infty$. The solutions are matched with the asymptotic solution at $y=-\infty$, by suitably adjusting the eigenvalue α.

3.1. *Asymptotic solutions*

In this subsection, solutions to equations (9)–(11) for $y\to\infty$ and $y\to-\infty$ are developed, by noting that the mean flow quantities attain constant values and their gradients vanish in the far field. The subscript 0 is used for the constant farstream values of the mean flow variables. From equation (11), it is clear that in the asymptotic limit, temperature fluctuations decouple from the velocity fluctuations, since $T'=0$. Defining

$$\omega^2\equiv\alpha^2+\frac{RePr}{(k/c_p)}\rho_0 i\alpha(U_0-c), \tag{12}$$

the solution to $\tilde{T}$ may be written as

$$\tilde{T}=\exp(\pm\omega y). \tag{13}$$

Substituting for $\tilde{u}$ and its higher derivatives from equation (3) into equation (9) and dropping terms involving mean flow gradients,

$$\tilde{v}^{iv}-\tilde{v}''(\gamma^2+\alpha^2)+\alpha^2\gamma^2\tilde{v}=\frac{(U_0-c)}{T_0}i\alpha(\tilde{T}'''-\gamma^2\tilde{T}'), \tag{14}$$

where γ is defined by

$$\gamma^2\equiv\alpha^2+\frac{Re}{\mu}\rho_0 i\alpha(U_0-c). \tag{15}$$

The temperature fluctuations act as a forcing term in this fourth-order inhomogeneous differential equation. There are two possible cases:

(a) $Pr=1$. In this case, $\omega^2=\gamma^2$. The homogeneous solutions are $\tilde{v}=\exp(\pm\alpha y)$ and $\tilde{v}=\exp(\pm\omega y)$, whereas the particular solution is 0.

(b) $Pr\neq1$. In this case, $\omega^2\neq\gamma^2$. The homogeneous solutions are given by $\tilde{v}=\exp(\pm\alpha y)$ and $\tilde{v}=\exp(\pm\gamma y)$. The particular solution is given by

$$\left[\frac{(U_0-c)}{T_0}\frac{1}{\omega^2-\alpha^2}\right]i\alpha\omega\exp(\omega y). \tag{16}$$

Only the $Pr=1$ case is considered in this paper.

3.2. *Numerical integration*

The numerical solution procedure involves integration of equations (9)–(11) by a shooting method using an eighth-order Runge–Kutta–Fehlberg algorithm, with a fixed step size. These equations are written as a system of seven coupled first-order differential equations. The vector of unknowns is

$$(\tilde{u},\tilde{v},\tilde{T},\tilde{u}',\tilde{u}'',\tilde{v}',\tilde{T}')^T.$$

The principal elements are given by the vector $(\tilde{u},\tilde{v},\tilde{T})^T$. As y_I approaches ∞ (subscript I stands for initial value), three linearly independent solutions are used to construct the principal vector as

follows:

$$\exp(-\alpha y_I)\begin{pmatrix} i \\ 1 \\ 0 \end{pmatrix} + B\exp(-\omega y_I)\begin{pmatrix} \frac{-i\omega}{\alpha} \\ 1 \\ 0 \end{pmatrix} + D\exp(-\omega y_I)\begin{pmatrix} \left(\frac{U_I - c}{T_I}\right) \\ 0 \\ 1 \end{pmatrix}, \tag{17}$$

where B and D are unknown linear combination constants. The three solutions are independently integrated to large negative y_F (subscript F for final integration station). The subscripts a, b and c will be used to indicate these three solution values at y_F. Thus, for instance,

$$\tilde{T}(y_F) = \tilde{T}_a + B\tilde{T}_b + D\tilde{T}_c. \tag{18}$$

Similar expressions may be written for the other variables. At the final station, solutions for $\tilde{v}$ and $\tilde{T}$ must have the asymptotic form:

$$\tilde{v} = C_1\exp(\alpha y_F) + C_2\exp(-\alpha y_F) + C_3\exp(\omega y_F) + C_4\exp(-\omega y_F), \tag{19}$$

$$\tilde{T} = C_5\exp(\omega y_F) + C_6\exp(-\omega y_F). \tag{20}$$

By differentiating equation (20) once and equation (19) thrice, and making use of equation (10), six independent equations can be obtained for the six coefficients appearing in equations (19) and (20). Expressions for C_2, C_4 and C_6 are important for the rest of this discussion and are given below:

$$C_2 = \frac{\exp(\alpha y_F)}{2\alpha(\omega^2 - \alpha^2)}(\tilde{v}''' - \alpha\tilde{v}'' - \omega^2\tilde{v}' + \alpha\omega^2\tilde{v}), \tag{21}$$

$$C_4 = \frac{\exp(-\omega y_F)}{2\omega(\alpha^2 - \omega^2)}(\tilde{v}''' - \omega\tilde{v}'' - \alpha^2\tilde{v}' + \alpha^2\omega\tilde{v}), \tag{22}$$

$$C_6 = \exp(\omega y_F)\left[\frac{\omega\tilde{T} - \tilde{T}'}{2\omega}\right], \tag{23}$$

wherein computed solutions of the form given by equation (18) should be used. Equations (19) and (20) require $C_2 = C_4 = C_6 = 0$ for finite solutions. Two of them can be made zero (here C_4 and C_6 were chosen) by appropriate choice of B and D at the final station. The result is

$$B = \frac{-H_a + [(\omega\tilde{T}_a - \tilde{T}'_a)/(\omega\tilde{T}_c - \tilde{T}'_c)]H_c}{H_b - [(\omega\tilde{T}_b - \tilde{T}'_b)/(\omega\tilde{T}_c - \tilde{T}'_c)]H_c}, \tag{24}$$

$$D = -\left[\left(\frac{\omega\tilde{T}_a - \tilde{T}'_a}{\omega\tilde{T}_c - \tilde{T}'_c}\right) + B\left(\frac{\omega\tilde{T}_b - \tilde{T}'_b}{\omega\tilde{T}_c - \tilde{T}'_c}\right)\right], \tag{25}$$

where H is defined as

$$H(\tilde{u}, \tilde{v}, \tilde{T}) \equiv \tilde{u}'' - \omega\tilde{u}' - i\alpha\tilde{v}' + i\alpha\omega\tilde{v} - \frac{(U_0 - c)}{T_0}(\tilde{T}'' - \omega\tilde{T}'). \tag{26}$$

The third condition (i.e. $C_2 = 0$) is satisfied iteratively by repeated integrations with suitably adjusted values of the eigenvalue α.

3.3. Pseudo-orthogonalization procedure

During the integration process, there is a tendency for the initially linearly independent solutions given by equation (17) to become linearly dependent. This will make it impossible to

match the linearly independent solutions at the other boundary. This problem becomes more severe at larger Reynolds numbers. Furthermore, the solutions undergo large amplification during the integration process (see Monkewitz[13]). Conventional Gram–Schmidt orthogonalization scheme will destroy the analytic dependence of the solutions on the initial conditions and parameters, making it difficult to iterate for the eigenvalue by repeated 'shooting'. A pseudo-orthognalization procedure is used both to preserve the linear independence of solution vectors and to maintain the analytic dependence of the solution on the initial conditions and parameters by controlling the magnitude of the solutions. This is based on the generalized method described by Monkewitz.[13] He was able to use this method successfully to solve the classical Orr–Sommerfeld problem.

Let **a**, **b** and **c** represent three complex solution vectors. Inner products and norms are defined by using the first two components of the vector. Thus, a pseudo-scalar product is defined as

$$(\mathbf{a}, \mathbf{b}) \equiv a_1 b_1 + a_2 b_2, \tag{27}$$

and the associated pseudo-norm as

$$|\mathbf{a}| \equiv \sqrt{(\mathbf{a}, \mathbf{a})}. \tag{28}$$

Since this particular choice does not involve complex conjugates, it guarantees that the final solution is analytically dependent on the initial conditions and parameters, thereby permitting its use in an iterative scheme to solve for the eigenvalue. The pseudo-orthogonalization steps (applied at each step during the integration) may be summarized as

$$\hat{\mathbf{b}} = \frac{\mathbf{b}}{|\mathbf{b}|}, \qquad \mathbf{a}^1 = \mathbf{a} - (\mathbf{a}, \hat{\mathbf{b}})\hat{\mathbf{b}}, \tag{29}$$

$$\mathbf{c}^1 = \mathbf{c} - (\mathbf{c}, \hat{\mathbf{b}})\hat{\mathbf{b}}, \qquad \hat{\mathbf{c}} = \frac{\mathbf{c}^1}{|\mathbf{c}^1|}, \tag{30}$$

$$\hat{\mathbf{a}} = \mathbf{a}^1 - (\mathbf{a}^1, \hat{\mathbf{c}})\hat{\mathbf{c}}. \tag{31}$$

Note that the pseudo-norm could be zero for a non-zero vector, creating a potential problem in the pseudo-orthogonalization steps described. Monkewitz[13] suggests remedies, including changing integration step size, or even completely skipping the pseudo-orthogonalization step at that point during the integration process. It was found that no such remedial action was required for the problems investigated in this paper.

The eigenvalue was obtained by an iterative procedure involving linear (when only results from two integrations are available) and quadratic (when three results are available) extrapolation, as described by Monkewitz.[13] In some instances, the eigenfunctions may be of value. For example, the eigenfunctions may be used in a direct numerical simulation to excite the flow at the most amplified frequency as in Mahalingam *et al.*[5] Once the eigenvalue is obtained, the eigenfunction may be reconstructed as follows. Let the subscript i represent the current integration station ($i=0$ at the first and $i=N$ at the final station). The desired solution at the final station is a linear combination expressed as

$$\mathbf{\Phi}_N = \hat{\mathbf{a}}_N + \hat{\mathbf{b}}_N B_N + \hat{\mathbf{c}}_N D_N. \tag{32}$$

The procedure used to compute B_N and D_N was described earlier in this section. Using the definitions for the pseudo-orthogonalized vectors, equation (32) may be written as

$$\mathbf{\Phi}_N = \mathbf{a}_N + \mathbf{b}_N B_{N-1} + \mathbf{c}_N D_{N-1}, \tag{33}$$

where the constants B_{N-1} and D_{N-1} are obtained as

$$B_{N-1}=\frac{B_N}{|\mathbf{b}_N|}-\frac{(\mathbf{a}_N,\hat{\mathbf{b}}_N)}{|\mathbf{b}_N|}+\frac{(\mathbf{a}_N^1,\hat{\mathbf{c}}_N)(\mathbf{c}_N,\hat{\mathbf{b}}_N)}{|\mathbf{c}_N^1\|\mathbf{b}_N|}-D_N\frac{(\mathbf{c}_N,\hat{\mathbf{b}}_N)}{|\mathbf{c}_N^1\|\mathbf{b}_N|}, \tag{34}$$

$$D_{N-1}=\frac{D_N}{|\mathbf{c}_N^1|}-\frac{(\mathbf{a}_N^1,\hat{\mathbf{c}}_N)}{|\mathbf{c}_N^1|}. \tag{35}$$

The above procedure is repeated for $i=N, N-1, \ldots, 0$. During the forward integration, all the required inner products in equations (34) and (35) are saved.

3.4. *Method of contour integration*

A problem in obtaining growth rate curves is the existence of more than one eigenvalue, α, for a fixed Reynolds number and frequency, β. Several modes may exist; for instance, there may be symmetric and anti-symmetric modes. The eigenvalues corresponding to these may lie close to each other in the α-plane. Thus, the iteration scheme could converge to either mode. There are also eigenvalues corresponding to higher modes (with large number of zero-crossings of the eigenfunction). This is especially true for damped and slightly amplified modes. The method of contour integration (see Lessen *et al.*[14]) is used to find the number of eigenvalues within a closed contour in the α-plane. The equation used to solve for the eigenvalue is

$$C_2(\alpha)=0. \tag{36}$$

For a prescribed closed contour Γ in the α-plane, the number of net multiples of 2π phase changes in the C_2 plane gives the number of zeros of equation (36). This is a consequence of the Cauchy integral theorem and the assumption that C_2 is an analytic function of α with no poles in Γ. The points in the α-plane at which the C_2 contour comes closest to the origin give good estimates of the eigenvalues.

4. RESULTS

Analytical expressions representative of premixed and non-premixed flames, for the mean flow (mean temperature and velocity) are assumed. Both cold and reacting flows involving large changes in temperature are examined. Figure 1 shows the neutral curve for the following mean, cold-flow profile:

$$U=U_0\tanh\left(\frac{y}{L}\right), \tag{37}$$

where U_0 and L are the velocity and length scales, respectively. This result was obtained from a temporal calculation and was primarily used to validate the numerical method. The agreement with Betchov and Szewczyk's[15] result is excellent. The curve of neutral stability is the same whether the analysis is temporal or spatial (see Betchov and Criminale[16]). All further cases in this section are based on spatial analysis.

4.1. *Premixed flames*

The first configuration considered is a premixed flame in a plane shear layer. Figure 2 shows neutral stability curves for cold flow as well as a shear layer with a temperature distribution typical of a premixed flame, with the velocity profile of the cold case. The following expressions were assumed for the profiles of mean velocity, U, and density, ρ. These are similar to those used

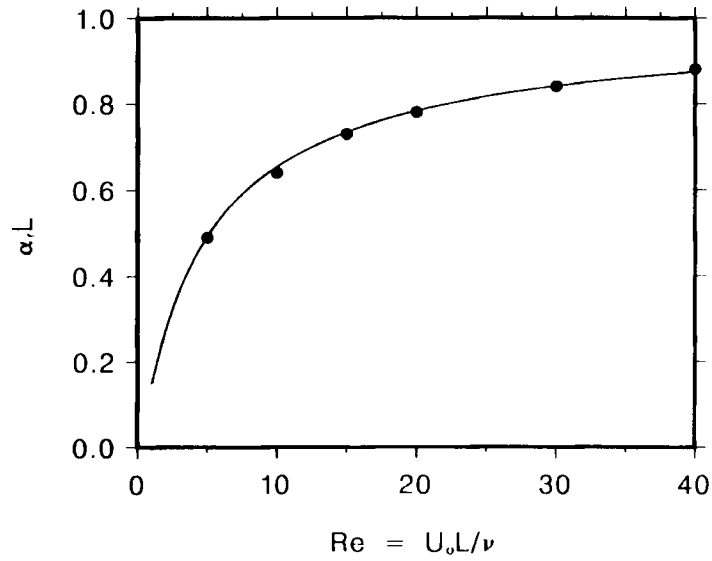

Figure 1. Neutral stability curve for $U = U_0$ tanh (y/L) (cold, non-reacting): (——) computed; (•) results from Reference 15

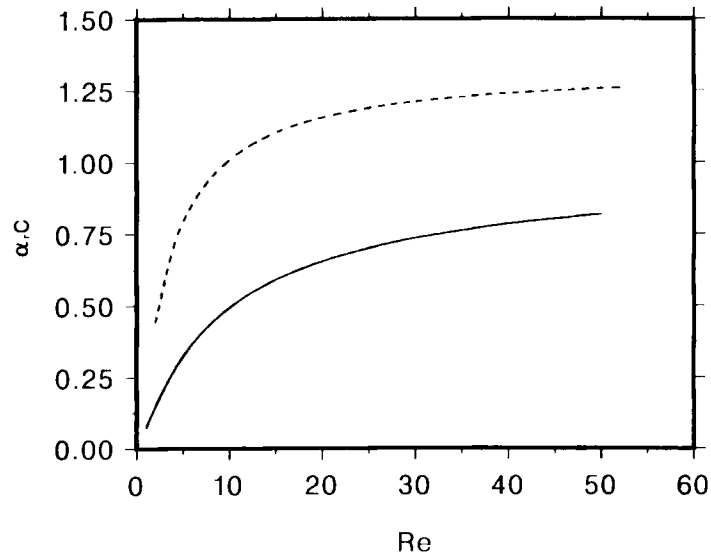

Figure 2. Neutral stability curve for premixed flame in a shear layer; $U = 1 + \tanh(y)$; $\rho = 3 + 2\tanh(y)$: (——) Cold; (-----) T ratio = 5·0

by Trouve *et al.*[4] in their inviscid analysis:

$$U = 1 + 0{\cdot}5 \tanh(y), \qquad \rho = 3 + 2\tanh(y). \tag{38}$$

The widths of the velocity and temperature profiles are the same. For planar flows, the necessary condition for the existence of instability is that $\rho U'$ vanish somewhere in the domain. For the

profiles chosen (heated case), this occurs at approximately $y=0{\cdot}275$ and the corresponding fluid velocity at that point is 1·13. The phase speed corresponding to the neutral disturbance approaches this value at large *Re*, consistent with inviscid theory. It is interesting to note that the neutral curve shifts outwards to higher frequencies, relative to the cold case. This result is consistent with the inviscid results for axisymmetric premixed flames, where the peak amplification rates as well as the frequency corresponding to the neutral stability point shift to higher frequencies (see Mahalingam *et al.*[5]). Frequency–Reynolds number combinations lying inside the neutral curve represent amplified disturbances, whereas those above the curve are damped. The critical Reynolds number is zero for both the cold and reacting flows. This is an important result, for it demonstrates that all the disturbances are amplified if the correct frequency is chosen.

4.2. Non-premixed flames

A non-premixed flame in a plane shear layer is now considered. The velocity and density profiles chosen are representative of such a configuration. Mean flow profiles of the following form were investigated:

$$U=1+0{\cdot}5\tanh(y), \qquad \rho=1-(1-\rho_{\min})\exp(-4y^2), \tag{39}$$

where $\rho_{\min}$ is the minimum density of the mean flow (the maximum being unity). For the case in which $\rho_{\min}=1/5$, the quantity $\rho U'$ vanishes at approximately $y=\pm 0{\cdot}61$ (corresponding $U=0{\cdot}72$ and 1·27) and at $y=0$ (corresponding $U=1$). However, only a single mode was found with a phase speed approaching unity at large Reynolds numbers. (This is not inconsistent since the condition for the existence of unstable disturbances is not a sufficient condition.) The resulting neutral curve is shown in Figure 3. The neutral frequency decreases with increasing heat release. This is consistent in trend with the inviscid results of Mahalingam *et al.*[5] The density profile has a characteristic width and its relation to the width of the velocity profile is an important parameter which was not investigated in detail.

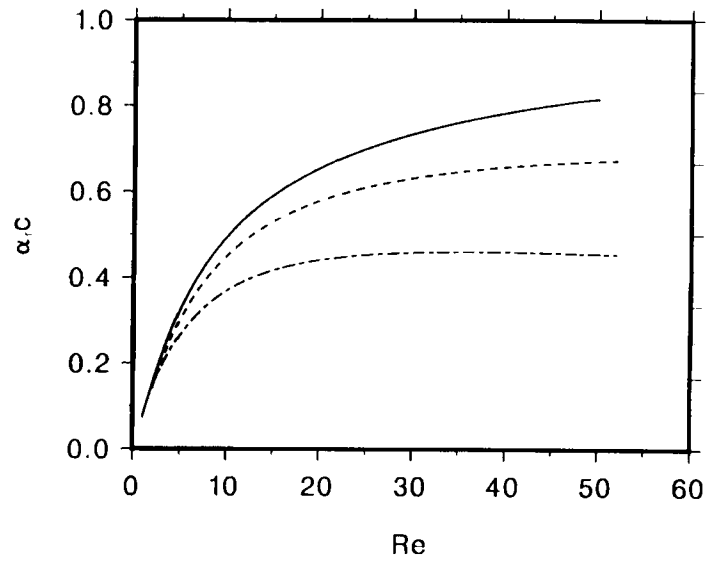

Figure 3. Neutral stability curve for non-premixed flame in a shear layer; $U=1+\tanh(y)$; $\rho=1-(1-\rho_{\min})\exp(-4y^2)$: (——) Cold; (-----) T ratio = 1·5; (—·—·—) T ratio = 5·0

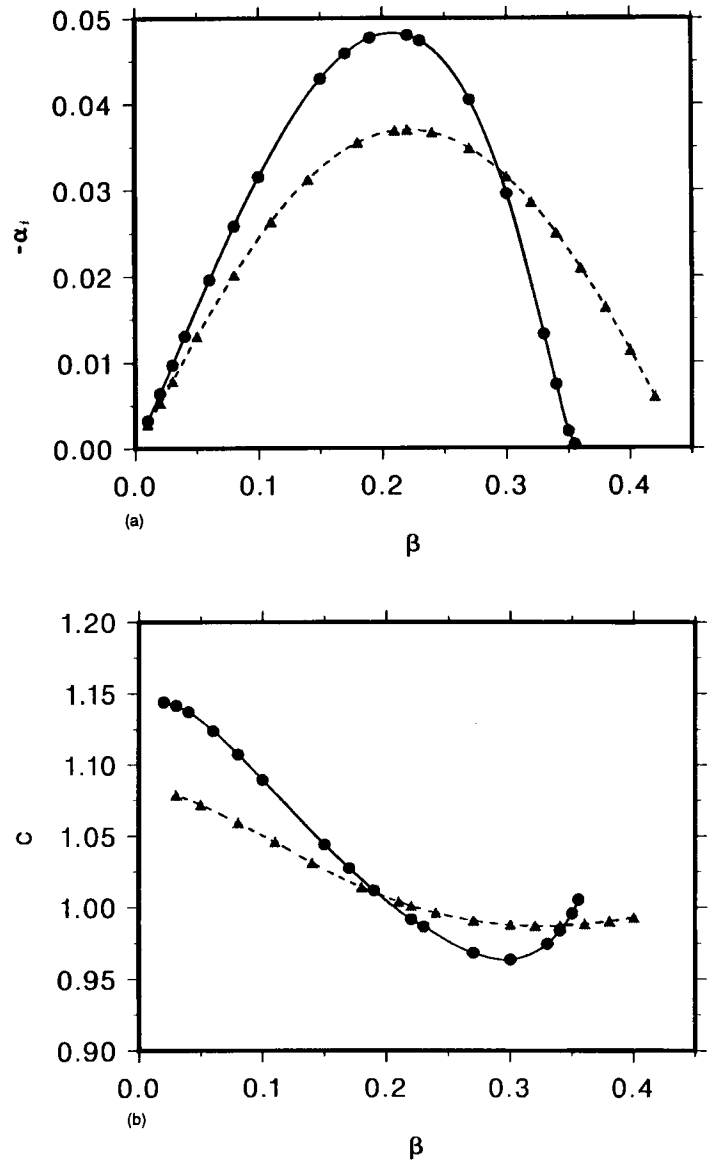

Figure 4. Effect of the Reynolds number on non-premixed flame stability. For $\rho_{min} = 1/5$ case of Figure 3: (a) Growth rate as a function of frequency; (b) phase velocity; (● —) $Re = 200$; (▲---) $Re = 30$

For the $\rho_{min} = 1/5$ case, the growth rate and phase velocity as functions of frequency at two different Reynolds numbers are shown in Figures 4(a) and 4(b). The change in the frequency corresponding to the most amplified mode is small. However, the peak growth rate is reduced by nearly 20% at the lower *Re*. At high frequencies, whereas the higher Reynolds number flow is stable, the lower one is unstable. It is known that decreasing the Reynolds number does not always result in a more stable flow (Lessen and Singh[17]). A similar behaviour was reported in axisymmetric cold flows by Morris[18]. He attributes it to the different behaviour of the kinetic

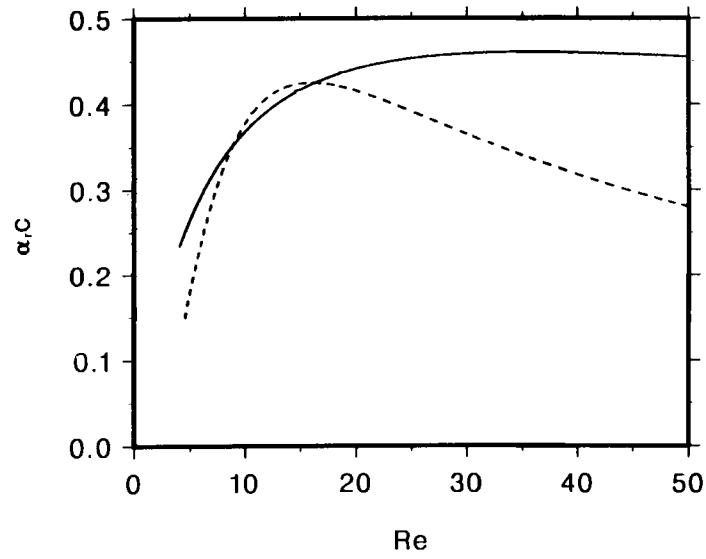

Figure 5. Neutral stability curve for non-premixed flame in a shear layer; $U=1+\tanh(y)$; $\rho=1-(1-\rho_{min})\exp(-4y^2)$, with T ratio of 5·0: (——) $\mu=$constant; (-----) $\mu=\mu(T)$ given by Sutherland law

energy production and dissipation mechanisms as functions of the Reynolds number. The phase velocity shows weaker variation at the lower Reynolds number so that the waves are less dispersive. These results show the importance of the Reynolds number. Although the Reynolds number based on cold flow may be sufficiently high for inviscid results to be applicable, a substantial reduction in the Reynolds number occurs in the region of the flame, and the viscous theory must be applied to understand the frequency response of the flow.

Results for non-constant viscosity

As mentioned above, the effect of changing viscosity through the flame is expected to be significant in terms of its influence on the neutral stability curve. Although the equations including the variation of viscosity with temperature are more complicated (see Appendix A), the same numerical procedure described in this paper is used to solve them. Figure 5 shows the neutral stability curves for a non-premixed flame ($\rho_{min}=1/5$ case) obtained assuming constant viscosity and when viscosity is allowed to vary with temperature according to Sutherland's law (see White[19]). A significant result is that, in either case, the critical Reynolds number approaches zero. The Reynolds number in either case is based on the vicosity at the highest temperature in the flow field.

5. CONCLUSIONS

The equations governing the viscous stability of low-speed reacting flows has been derived. A 'shooting' method, combined with an iterative procedure has been adapted to solve the resulting equations. The method accurately reproduces the neutral stability curve for a planar, constant-density, shear layer. The neutral curve shifts outwards towards higher frequencies for premixed flames in shear layers. However, for non-premixed flames, the shift is towards lower

frequencies. These results are for a constant viscosity. The method developed in this paper is used to allow for a prescribed variation of viscosity with temperature. The results indicate that the critical Reynolds number is zero for both constant and varying viscosity cases.

ACKNOWLEDGEMENTS

The author is grateful to J. H. Ferziger and B. J. Cantwell for many valuable discussions during the initial phase of this work. F. Hirt helped the author understand the intricacies associated with solving the classical Orr–Sommerfeld problem and also provided a computer code, inherited by him from M. A. Monkewitz, that was subsequently modified to handle reacting flows. The author expresses his sincere thanks to N. Sullivan who generated the figures in this paper. The computing facility provided by NASA Ames/Stanford Center for Turbulence Research is gratefully acknowledged. The author acknowledges the start-up funds provided by the University of Colorado that helped complete this work.

APPENDIX

When viscosity is allowed to vary with temperature, the following equations replace equations (9) and (11), respectively:

$$\tilde{u}''' = \frac{\rho Re i\alpha}{\mu}\left[(U-c)\tilde{u}' - i\alpha(U-c)\tilde{v} + U'\tilde{u} + \frac{\rho'}{\rho}(U-c)\tilde{u} + \frac{1}{i\alpha}\left(U'\tilde{v}' + U''\tilde{v} + \frac{\rho'}{\rho}U'\tilde{v}\right)\right] + \alpha^2\tilde{u}' - i\alpha^3\tilde{v} + i\alpha\tilde{v}'' - \frac{\mu'}{\mu}(\tilde{u}'' - 2\alpha^2\tilde{u}) - \frac{\mu''}{\mu}(\tilde{u}' + i\alpha\tilde{v}) - \frac{\tilde{\mu}}{\mu}(\alpha^2 U' + U''') - \frac{\tilde{\mu}'}{\mu}2U'' - \frac{\tilde{\mu}''}{\mu}U' \tag{40}$$

and

$$\tilde{T}'' = \frac{RePr}{(k/c_p)}\rho[\tilde{T}i\alpha(U-c) + T'\tilde{v}] + \alpha^2\tilde{T} - \frac{(\tilde{k}/c_p)}{(k/c_p)}T', \tag{41}$$

where $\tilde{\mu}$ and $\tilde{k}/c_p$, represent fluctuating quantities. Since $\mu = \mu(T)$, the quantities μ', μ'', etc., can be readily obtained. Similarly, the fluctuating quantities $\tilde{\mu}$, $\tilde{\mu}'$, etc., are related to $\tilde{T}$ and T. Note that equation (10) remains unchanged.

REFERENCES

1. I. Kimura, 'Stability of laminar jet flames', *Proc. 10th Int. Symp. on Combustion*, The Combustion Institute, Pittsburgh, 1965, pp. 1295–1300.
2. A. J. Grant and J. M. Jones, 'Low-frequency diffusion flame oscillations', *Combust. Flame*, **25**, 153–160 (1975).
3. J. Buckmaster and N. Peters, 'The infinite candle and its stability—a paradigm for flickering diffusion flames', *Proc. 21st Int. Symp. on Combustion*, The Combustion Institute, Pittsburgh, 1986, pp. 1829–1836.
4. A. Trouve, S. M. Candel and J. W. Daily, 'Linear stability of the inlet jet in a ramjet dump combustor', *AIAA Paper No. AIAA-88-0149*, 1988.
5. S. Mahalingam, B. J. Cantwell and J. H. Ferziger, 'Stability of low speed reacting flows', *Phys. Fluids A*, **3**, 1533–1543 (1991).
6. T. L. Jackson and C. E. Grosch, 'Inviscid spatial stability of a compressible mixing layer. Part 2. The flame sheet model', *J. Fluid Mech.*, **217**, 391–420 (1990).
7. S. A. Maslowe and R. E. Kelly, 'Inviscid instability of an unbounded heterogeneous shear layer', *J. Fluid Mech.*, **48**, 405–415 (1971).
8. M. M. Koochesfahani and C. E. Frieler, 'Inviscid instability characteristics of free shear layers with non-uniform density', *AIAA Paper No. AIAA-87-0047*, 1987.

9. P. A. McMurtry, J. J. Riley and R. W. Metcalfe, 'Effects of heat release on the large scale structure in turbulent mixing layers', *J. Fluid Mech.*, **199**, 297–332 (1989).
10. S. Mahalingam, B. J. Cantwell and J. H. Ferziger, 'Full numerical simulation of coflowing, axisymmetric jet diffusion flames', *Phys. Fluids A*, **2**, 720–728 (1990).
11. P. G. Drazin and W. H. Reid, *Hydrodynamic Stability*, Cambridge University Press, Cambridge, 1981.
12. M. R. Malik, 'Numerical methods for hypersonic boundary layer stability', *J. Comput. Phys.*, **86**, 376–413 (1990).
13. M. A. Monkewitz, 'Analytic pseudoorthogonalization methods for linear two-point boundary value problems illustrated by the Orr–Sommerfield equation', *J. Appl. Math. Phys. (ZAMP)*, **29**, 861–870 (1978).
14. M. Lessen, S. G. Sadler and T. Y. Liu, 'Stability of pipè Poiseuille flow', *Phys. Fluids*, **11**, 1404–1409 (1968).
15. R. Betchov and A. B. Szewczyk, 'Stability of a shear layer between parallel streams', *Phys. Fluids*, **6**, 1391–1396 (1963).
16. R. Betchov and W. O. Criminale, *Stability of Parallel Flows*, Applied Mathematics and Mechanics Series, Vol. 10, Academic Press, New York, 1967.
17. M. Lessen and P. J. Singh, 'The stability of axisymmetric free shear layers', *J. Fluid Mech.*, **60**, 433–457 (1973).
18. P. J. Morris, 'The spatial viscous instability of axisymmetric jets', *J. Fluid Mech.*, **77**, 511–529 (1976).
19. F. M. White, *Viscous Flow*, McGraw-Hill, New York, 1974.